



Simple and low-cost solution method for cobalt doped CuO nanostructured powder

Samed Çetinkaya ^{*1}, Selma Erat ¹, Murat Aycibin ¹

¹Mersin University, Department of Medical Services and Techniques, Mersin, Türkiye, samedcetinkaya@mersin.edu.tr, selma.erat@mersin.edu.tr, murataycibin@mersin.edu.tr

Cite this study: Çetinkaya, S., Erat, S., & Aycibin, M. (2023). Simple and low-cost solution method for cobalt doped CuO nanostructured powder Advanced Engineering Science, 3, 188-195

Keywords

Cobalt
CuO
CBD
Impurity Level
Microplate

Research Article

Received:28.09.2023
Revised: 21.10.2023
Accepted:28.10.2023
Published:03.11.2023



Abstract

In present work, pure and Co doped nanostructured powder were fabricated by chemical bath deposition method. X-ray analysis reveals that both pure and Co doped CuO have monoclinic crystal structure. After introducing Co²⁺ ions into the host, the crystalline percentage was decreased. The dislocation density and the microstrain were increased with Co addition. It is observed that pure CuO has nanoplate-assembled structure whereas CuO:Co nanostructured powder has irregular microplate-like particles. Besides, Cu, Co, and O peaks are observed in EDX spectrum. The optical band gap energy reduced from 1.62 to 1.59 eV after CuO doped with Co. The electrical activation energy values were calculated for both pure and Co doped CuO as 0.134 eV and 0.232 eV, respectively.

1. Introduction

In recent years, researchers have been working on rearranging the boundaries of technology with newly developed nanostructured materials. Currently, it has been possible to develop enormous number of new materials via development of nanotechnology. Due to their optical, electrical and structural properties, in recent years, the nanostructured materials like SnO₂, ZnO and CuO have gotten researchers attention for technological application opportunity such as superconductors, solar cells, photocatalytic degradation, gas sensors and biosensors [1]. Among various metal oxides, copper oxide (CuO) has emerged as the most versatile host for dopant elements due to its plethora of applications and scientific point of view [2]. Moreover, CuO has been shown valuable materials in the industrial applications such as gas sensors, magnetic storage medium, solar energy transfers and semiconductors [3]. CuO is a p-type semiconductor with a bandgap ranging from 1.85 eV to 2.00 eV, which is the acceptable range for solar energy applications.

With dopant elements, it is possible to make change on properties of semiconductors and develop new functional nanomaterials [4]. Therefore, many researches have researched to investigate the effect of transition metal (TM) like Ni, Mn, Fe, Pb and Ag elements on electrical, optical and structural properties of CuO nanoparticle. Ponnar et al. used Ce as a dopant element and revealed its effects on properties of CuO [5]. Borzi and his friends investigated the magnetism of CuO: Fe [6]. The effects of dopant element of La on the photoluminescence properties and lattice defects of CuO was investigated [7]. Meneses and his friends used co-precipitation methods to grow Cu_{1-x}TM_xO (TM= Ni, and Fe) sample to investigated its temperature dependent structural and magnetic properties [8]. Al doped CuO was produced by the microwave chemical route to reveal its structural and thermoelectrical properties [9]. Goyal et al. used Zn as a dopant element for CuO and investigated effects of Zn on the properties of CuO synthesized with low-temperature co-precipitation method [10]. Bayansal and his friends investigated effect of Co on the structural, morphological, and optical properties of CuO NSP [11]. Ocak et al. used Ni as a dopant element to modify electrical and optical properties of CuO [12]. Influence of Mn-doping on the photocatalytic solar cell efficiency of CuO nanowires was investigated and revealed [13]. Gaur et al. reported some

physical properties of CuO after doped with various Li concentrations [14]. Oxygen evolution reaction of a CuO after doped with Co was reported by Sun et al [5]. Ferromagnetism of CuO doped with Fe at room temperature was investigated [15].

Reported studies in the literature reveals that when the dopant ions have smaller ionic radius than replacing ions in host materials, the conductivity of material increases and this phenomenon is still under investigations [14]. In this study, we used Co^{2+} as a dopant element, which has smaller ionic radius, 0.065nm than that of Cu^{2+} (0.073nm) [5], to investigate its effects on structural, electrical, morphological and optical properties of CuO.

2. Material and Method

2.1. Materials

All chemicals used in the experiments were of analytical grade and were used as received without any further purification. Copper (II) chloride dehydrate ($\text{CuCl}_2 \cdot 2\text{H}_2\text{O}$) and Cobalt (II) chloride hexahydrate were purchased from Sigma-Aldrich and Ammonia solution (NH_4OH) was purchased from Merck KGaA.

2.2. Preparation of nanostructures

Pure and Cobalt doped CuO nano-structured powders (NSP) were grown by an aqueous precursor solution method. Chemical bath deposition (CBD) method is a cost effective and relatively low temperature method (25–90 °C) that allows to deposit large scale semiconductor NSP [16]. Copper (II) chloride dehydrate ($\text{CuCl}_2 \cdot 2\text{H}_2\text{O}$) (0.1 M) and cobalt (II) chloride hexahydrate ($\text{CoCl}_2 \cdot 6\text{H}_2\text{O}$) were used as source precursors for CuO films and Co-dopant, respectively.

Briefly, CuO NSP were fabricated in a beaker (100mL) from a mixture of 0,1 Molar a Copper (II) chloride dehydrate ($\text{CuCl}_2 \cdot 2\text{H}_2\text{O}$, $\geq 98\%$), Ammonia solution and distilled water at room temperature. The solution was stirred for 15 minute to obtain completely dissolved homogenous precursor solution. The initial pH value was adjusted to ~ 10 by using an aqueous ammonia solution, for all precursors under constant stirring. A light blue precipitate of $\text{Cu}(\text{OH})_2$ was yielded. Then, the color of the solution changes into the dark blue after boiled at $\sim 90^\circ\text{C}$. Heating rate was $10^\circ\text{C}/\text{min}$., and it took about 10 min to boil the solution. Therefore, it was transformed from $\text{Cu}(\text{OH})_2$ to CuO. This transformation can occur in ambient conditions by thermal dehydration at a relatively low temperature [17]. After 20 min. boiling process, the solution was kept at room temperature for 3h for the copper oxide precipitates to deposit at the bottom of the beaker. After the obtained deposit of the CuO, powder was washed by ethanol and double distilled water, and then, sample was left to dry at 100°C in an oven for 12h. After this process, sample was annealed in a furnace for 1 h at 500°C to achieve a uniform CuO structure. Similarly, Cobalt doped CuO nanostructures have been prepared by adding a cobalt nitrate hexahydrate ($\text{Co}(\text{NO}_3)_2 \cdot 6\text{H}_2\text{O}$, $\geq 99\%$) with volume of 2.5 mL. The samples were labeled within the text as follows: P0: pure CuO and P1: 2.5% Cobalt doped CuO. The CuO and CuO:Co thin films were produced on glass substrate using doctor blading method for optical properties measurements.

2.3. Characterization Techniques

The crystallographic structure of the CuO and CuO: Co nanostructured powder (NSP) was characterized by an X-ray diffractometer (XRD, Rigaku Smartlab X-Ray diffractometer, Tokyo, Japan) using $\text{Cu K}\alpha$ radiation ($\lambda = 1.54059 \text{ \AA}$) in steps of 0.01° within the 2θ range of $20\text{--}80^\circ$ at room temperature.

In addition, the surface morphology of the films has been studied using scanning electron microscopy (SEM) and Energy Dispersive X ray (EDXS) spectroscopy (SEM, ZEISS EVO-LS10, NTS, Munich, Germany). The CuO and CuO:Co nanostructured powder were pressed into the disks (diameter:10 mm, thickness: 12 mm) under the pressure of 75 MPa using manual press (MSE Technology, Türkiye) and sintered at 350°C , 1h for electrical resistivity measurements. The electrical properties of the disks were investigated using the two-point probe method in the temperature range of 300–540 K using a homemade Labview program and a computer-interfaced GW Instek multimeter, GPD 4303S (New Taipei, Taiwan) with high accuracy and a voltage source. The optical absorption and refraction spectra of the pure and cobalt doped CuO thin films were analyzed using an UV-Vis spectrophotometer at the wavelength range of 200–1100 nm.

3. Results and Discussion

3.1. Crystallographic structure of CuO and CuO:Co nanostructured powder

The phase and crystallinity properties of pure and Co doped CuO NSP were analyze with Powder X-Ray Diffractometer (PXRD). Figure 1 illustrates the PXRD patterns of chemically deposited NSP. All diffraction peaks match the monoclinic CuO phase (ICCD: 801916) and no any other peaks and/or a secondary phase were observed. These results are good agreement with the literature [1, 18–21].

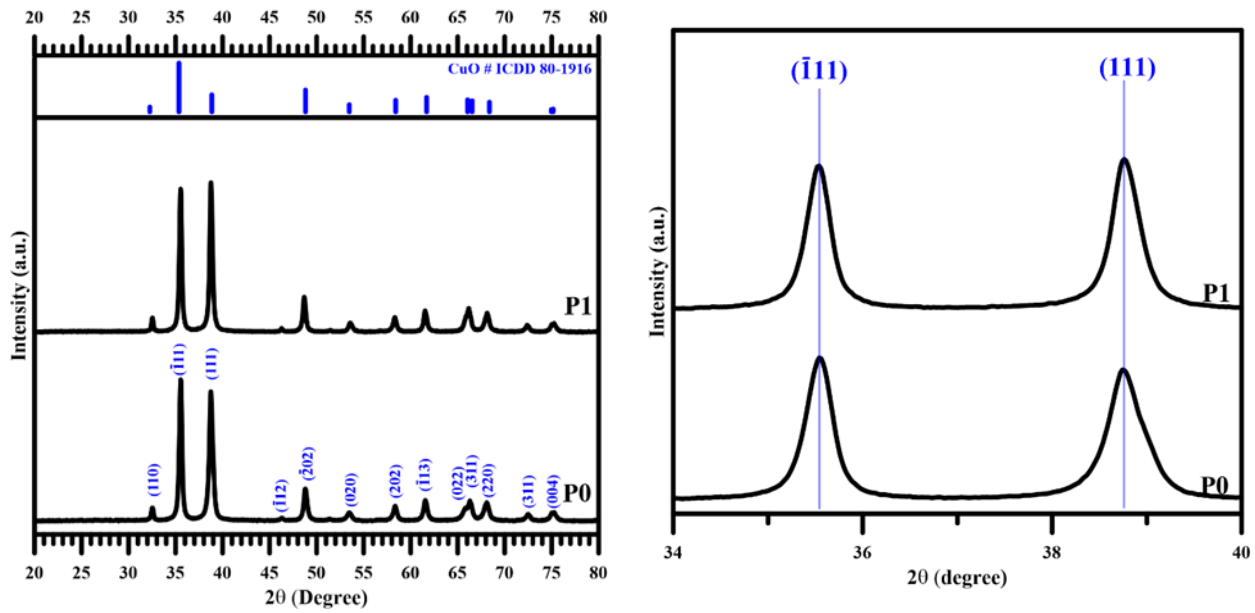


Figure 1. XRD diffractograms (left) and enlarged $(\bar{1}11)$ and (111) peaks (right) of the pure and the Co doped CuO NSP.

In **Figure 1**, it was determined that the diffraction peaks with $(\bar{1}11)$ and (111) preferred orientation belonging to the P0 sample belong to monoclinic CuO. Apart from these, (110) , $(\bar{2}02)$, (020) , (202) , $(\bar{1}13)$, (022) , (113) , (311) and (004) peaks were also observed. **Figure 1** shows the variation in diffraction peak intensity due to Cobalt ion addition.

Additionally, it was determined that $(\bar{1}11)$ and (111) peak positions did not undergo a large shift with Co concentration (**Table 1**). Additionally, the crystallinity percentage values calculated for two samples are given in **Table 1**. Crystallinity is defined as the periodic arrangement and degree of structural order of atoms or molecules in a solid. Moreover, the degree of crystallinity can be calculated from the area of crystalline peaks and amorphous peaks using the following relationship [22] (**Equation 1**).

Table 1. Some structural parameters obtained and calculated from the films (D, crystallite size; ϵ , micro strain; ρ , dislocation density; d, distance between planes and crystallinity).

Sample ID	$(\bar{1}11)$		(111)		(020)		D (nm)	ϵ $\times 10^{-4}$	$\rho \times 10^{19}$ (cm^{-2})	Crystallinity (%)
	2θ (deg.)	$d(\lambda)$	2θ (deg.)	$d(\lambda)$	2θ (deg.)	$d(\lambda)$				
P0	35.53	2.524	38.71	2.324	53.44	1.713	24.69	15.61	1.99	96.16
P1	35.52	2.525	38.73	2.323	53.53	1.710	20.10	18.57	2.72	91.01

$$\text{crystallinity degree}(\%) = \frac{(\text{total area of crystalline peaks})}{(\text{total area of all peaks})} \quad (1)$$

According to these values in **Table 1**, it was observed that the crystallinity percentage decreased with the Co concentration. The Co doping process for the CuO is likely to cause defects in the CuO structure that will reduce the crystallinity of the film after doping process. In **Figure 1**, PXRD data showed that the peak intensities decreased with cobalt doping (2.5%).

As listed in **Table 1**, the crystal size was calculated to be 24.69 and 20.10 nm at 0.0 and 2.5 wt% Cobalt concentration, respectively. Accordingly, a decrease in crystallite size was observed with the addition of cobalt. In this study, it has been observed that the dislocation density and strain increase as the crystallite size of CuO decreases, the reason is the increase in the surface/volume ratio in the nanoregion [1,23].

The average crystallite size (D) is calculated from the full width of the half maximum (FWHM) of a peak (β) using the Scherrer formula, (**Equation 2**):

$$D = \frac{0.94\lambda}{\beta \cos \theta} \quad (2)$$

Here " λ " is the wavelength of the X-ray radiation, " θ " is the Bragg diffraction angle and " β " is the angular width of the peaks in FWHM [1]. The decrease in crystallinity percentage values can be attributed to the increase in the crystallinity of NSP. The defect density, which gives the number of defects in the structure, is given in Equation 3 [1].

$$\delta = 1/D^2 \tag{3}$$

Low values of defect location density indicate the presence of crystallized traps. The micro tension (ε) of the films is calculated using Equation 4 [1]:

$$\varepsilon = \frac{\beta \cos \theta}{4} \tag{4}$$

Microballs are caused by the ion size difference between the dopant (Co, doped) element and the host (Cu, resident) element (Figure 2). As a result of cobalt doping, it was observed that the microstrain and dislocation density values increased. The crystallization process in nanostructures can trigger changes in microstrain and dislocation density due to differences in the ionic sizes of host and dopant elements [24]. Therefore, this implies that there is a clear relationship between crystallite size, microstrain, dislocation density and cobalt concentration. Additionally, when the SEM images were examined, it was seen that the nanostructured micro-sized plates tended to shrink as a result of the Cobalt additive. Consequently, the formation of smaller crystals may result from an increased density of nucleation centers.

3.2. Morphological Properties and Elemental Analysis of CuO and CuO:Co nanostructured powder

In Figure 2, P0 presents the SEM image of pristine CuO microspheres, which shows the nanoplate-assembled microspheres with a plate interior structure. Similar morphologies were reported by Zhao et al [25] and Bayansal et al. [26]. To have an insight into the morphology evolution induced by different incorporating content of Co in the CuO, the FESEM images at various magnification are collected.

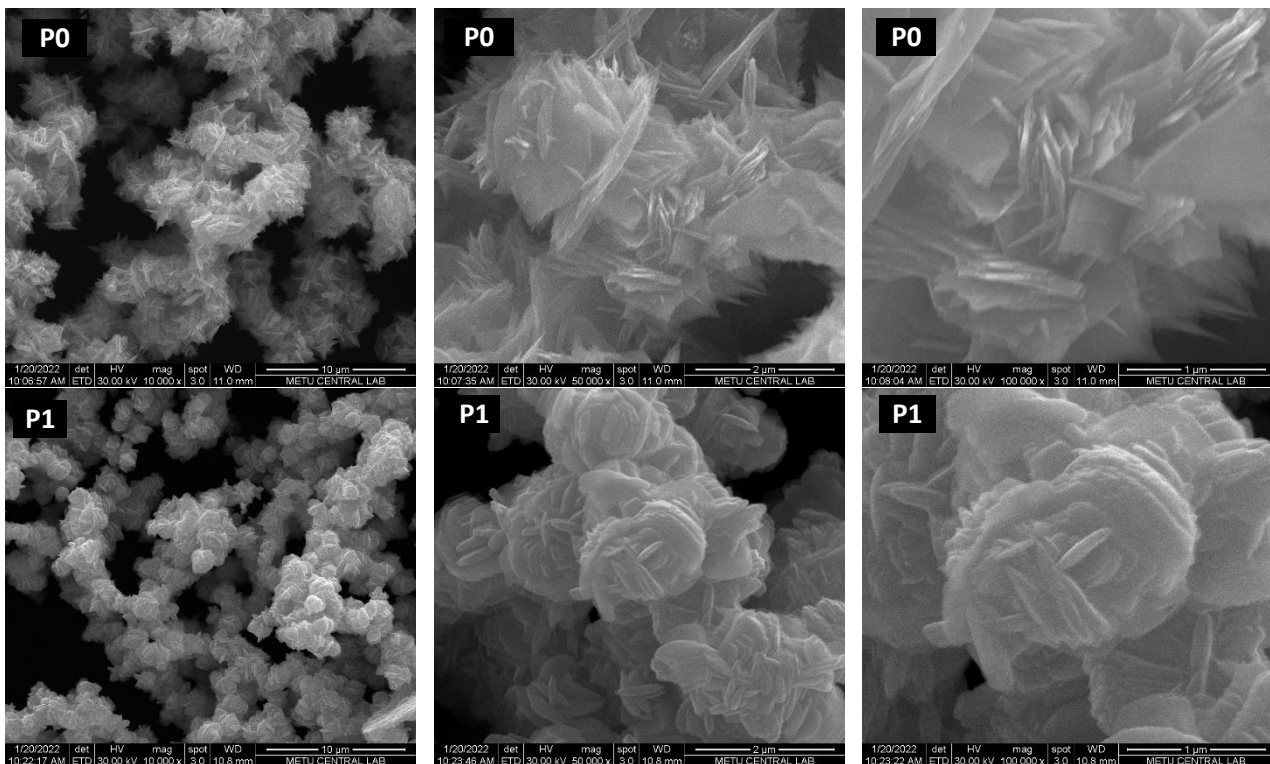


Figure 2. The variety magnifications surface morphology of the pure and Co doped CuO NSP.

On the other hand, the dimensions of these CuO microplates were determined to decrease (from ~700 nm to ~400 nm) with increase of the dopant. As shown in Figure 2, P(1), when the volume of precursor solution of Co is increased up to 2.5 mL, thus, it can be concluded that the surface properties of CuO nanostructures change significantly once the Co ions introduced. In addition, according to the FESEM images, it was observed that with the introducing the Co ions, irregular microplate-like particles were formed. Munir et al. [27] reported similar result. The distribution of individual elements in the nanocomposites can be demonstrated by the EDX analysis

given in the Figure 3. In the EDX spectrum, the peaks of Cu, Co and O elements are observed. It can be interpreted from the obtained results that Co doping has a significant effect on the morphological properties of the CuO films.

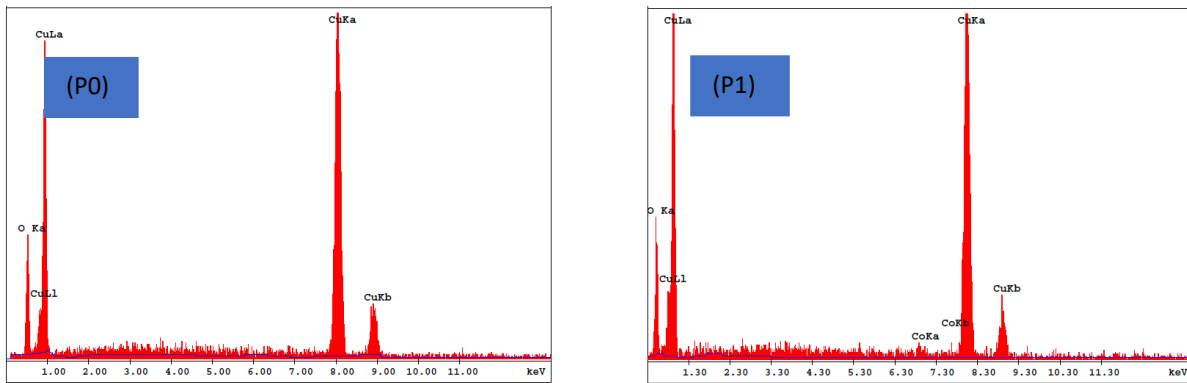


Figure 3. Energy dispersive X-ray spectroscopy (EDS) spectrum of pure and Co doped CuO NSP.

The EDX spectrum shows the presence of Cu (81.005 wt %) and O (18.995 wt %) elements in pure CuO nanostructure and the chemical elements of Co (2.421 wt %), Cu (73.825 wt %), and O (23.745 wt %) for the Co doped CuO. The EDX results approved the successful synthesis of the Co-doped CuO.

3.3. Optical Properties of CuO and CuO:Co Thin Films

The absorbance spectra of pure and Co doped CuO thin films were measured using UV-Vis spectrophotometer in the wavelength region of 200-1100 nm. Both of the films were subjected to thermal treatment (350°C, 1h) before the measurements. The band gap energy values were calculated using the fundamental absorptions, which correspond to electron excitation from the valance band to the conduction band [11]. Tauc plots of NSP as a function of Co contribution were shown in Figure 5. The optical band gap energies of the films were calculated by using the Equation 5.

$$\alpha h\nu = A(h\nu - E_g)^n \tag{5}$$

where A is a constant, α is the optical absorption coefficient, and n is 1/2 for indirect transition. The linear part of the Tauc graphs shown in Figure 4 is used to calculate the bandgap value of the films [28]. It is obvious that once Co ions are introduced into the host material, CuO, the electronic band structure of the material is changed. The optical band gap is reduced with 2.5% Co addition. The optical band gap energies of the NSP calculated as 1.62 and 1.59 eV for CuO and CuO:Co, respectively (Figure 4). The values of the optical band gap are in agreement with the literature [29].

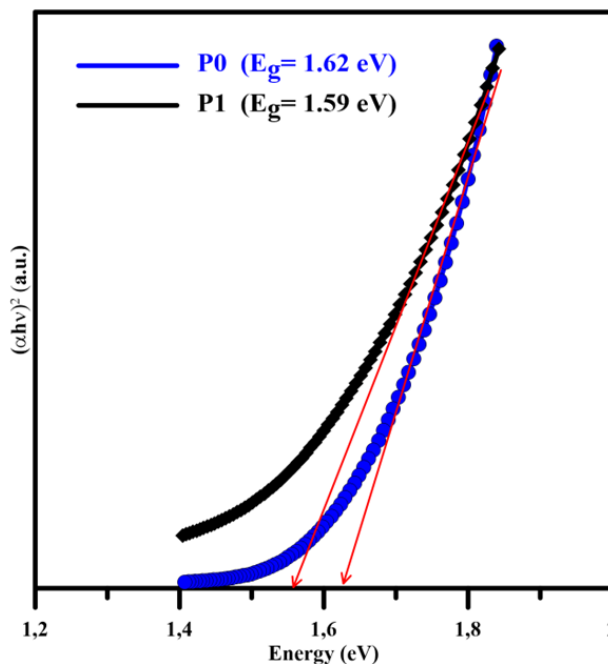


Figure 4. Tauc plots of pure and Co doped CuO NSP.

3.4. Electrical properties of the CuO and CuO:Co Disks

The CuO and CuO:Co nanostructured powders were pressed into the disks (diameter:10 mm, thickness: 12 mm) under the pressure of 75 MPa and sintered at 350°C for 1h. The electrical resistivity of the disks was measured using LabVIEW graphical programming language and programmable precision multimeter (GW Instek 8261A) and Voltage source (GW Instek 4303S) equipment. Using the developed software, the conductivity-temperature properties of the disks investigated in the temperature range of 300-500 K. the conductive spring contact tips used in the two-contact method are used in FEIN brand and scientific circuit conductivity testing (ICT) processes. These are gold-plated contact tips with a diameter of 0.6 mm, low contact resistance, and stable measurements between (-)45° and +200°C.

According to the solid-state theory of semiconductors, the temperature dependence of the dark electrical resistance of a semiconductor with one or more impurity levels. The ionization energy values of impurity levels calculated using equations in our previous report and the energy levels calculated as P0: 0.134 and P1: 0.232 eV, respectively. The change in activation energy values for the pure and cobalt doped NSP given in Figure 5.

The activation energy level represents the energy difference between the acceptor level and the valence band. Therefore, the amount of energy required for the charge carriers located in these intermediate levels (impurity) between the valence and conductivity energy levels to pass into the conduction band and contribute to the electrical conductivity can be calculated using the temperature-dependent current voltage measurement technique.

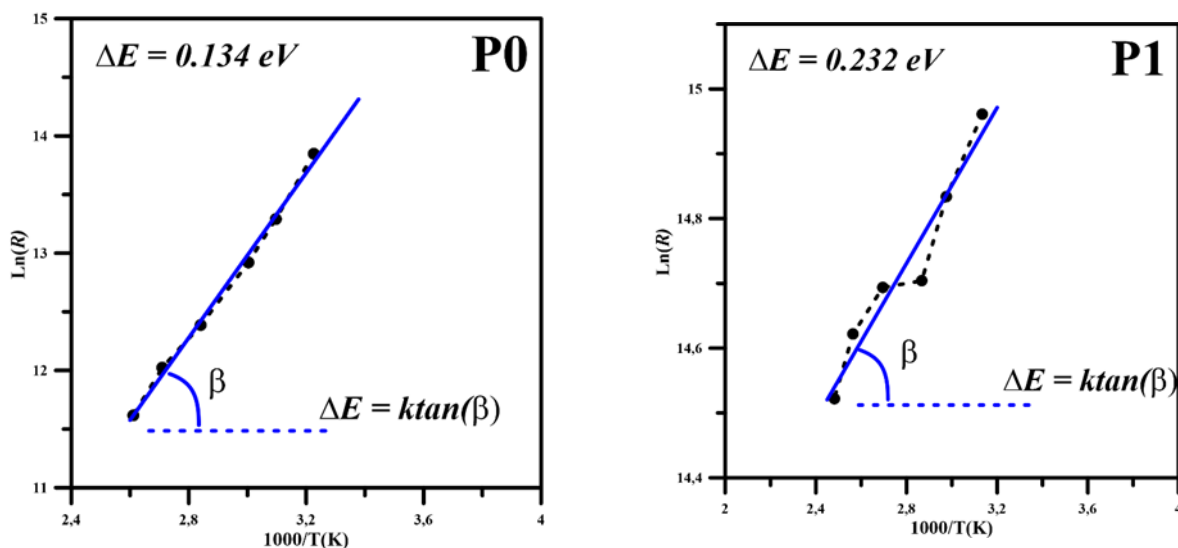


Figure 5. Variations of impurity levels for the pure and Co doped CuO thin films.

The activation energy level values (Figure 5) increased within the dopant element. The CuO semiconductor used in our study has p-type electrical conductivity. For this reason, it can be interpreted that the increase in carrier concentration will decrease the Fermi Energy level in the E_g energy region and this may cause an increase in the activation energy which are compatible with the literature [30].

4. Conclusion

The X-ray diffraction analysis shows that CuO and CuO:Co nanostructured powders have monoclinic crystal structure. The crystallinity percentage decreased with introducing Co^{2+} ions into the host material. The crystal size was calculated to be 24.69 and 20.10 nm for pure and 2.5 (wt)% Co doped CuO, respectively. It was observed that the microstrain and dislocation density values increased with cobalt addition. The crystallization process in nanostructures can trigger changes in microstrain and dislocation density due to differences in the ionic sizes of the host and dopant elements. FESEM results show that CuO and CuO:Co nanostructured powder forms the nanoplate-assembled structure. According to the FESEM analysis, introducing Co^{2+} ions cause irregular microplate-like particles to be formed. In the EDX spectrum, it was observed that there were peaks of Cu, Co and O elements. The absorbance measurements were taken using UV-Vis spectrophotometer, the band gap energy values were calculated as 1.62 and 1.59 eV for CuO and CuO:Co, respectively. Finally, the electrical activation energy values of impurity levels calculated as P0: 0.134 and P1: 0.232 eV. Due to the p-type electric conductivity of CuO, the increase in carrier concentration will decrease the Fermi energy level in the optical band gap energy range and this may cause an increase in the activation energy. Doping CuO with Co^{2+} ions affect the morphological, optical and electrical properties significantly whereas it doesn't change crystallographic structure.

Funding

This research received no external funding.

Author contributions

Samed Çetinkaya: Conceptualization, Methodology, Software, Writing-Original draft preparation **Selma Erat:** Data curation, Writing-Original draft preparation, Validation. **Murat Aycibin:** Visualization, Writing-Reviewing and Editing.

Conflicts of interest

The authors declare no conflicts of interest.

References

1. Maini, A., & Shah, M. A. (2021). Investigation on physical properties of nanosized copper oxide (CuO) doped with cobalt (Co): a material for electronic device application. *International Journal of Ceramic Engineering & Science*, 3(4), 192-199. <https://doi.org/10.1002/ces2.10097>
2. Kaur, M., Prasher, D., & Sharma, R. (2022). Recent developments on I and II series transition elements doped SnO₂ nanoparticles and its applications for water remediation process: a review. *Journal of Water and Environmental Nanotechnology*, 7(2), 194-217. <https://doi.org/10.22090/JWENT.2022.02.007>
3. Srivastava, S., & Agarwal, A. (2018). Influence of Co doping on structural and optical properties of CuO nanoparticles. *Journal of Ovonic Research*, 14(5), 395-404.
4. Rahman, A. S., Islam, M. A., & Shorowordi, K. M. (2015). Electrodeposition and characterization of copper oxide thin films for solar cell applications. *Procedia Engineering*, 105, 679-685. <https://doi.org/10.1016/j.proeng.2015.05.048>
5. Renaudin, G., Gomes, S., & Nedelec, J. M. (2017). First-row transition metal doping in calcium phosphate bioceramics: A detailed crystallographic study. *Materials*, 10(1), 92. <https://doi.org/10.3390/ma10010092>
6. Borzi, R. A., Stewart, S. J., Punte, G., Mercader, R. C., Curutchet, G. A., Zysler, R. D., & Tovar, M. (2000). Effect of ion doping on CuO magnetism. *Journal of Applied Physics*, 87(9), 4870-4872. <https://doi.org/10.1063/1.373186>
7. Devi, L. V., Selvalakshmi, T., Sellaiyan, S., Uedono, A., Sivaji, K., & Sankar, S. (2017). Effect of La doping on the lattice defects and photoluminescence properties of CuO. *Journal of Alloys and Compounds*, 709, 496-504. <https://doi.org/10.1016/j.jallcom.2017.03.148>
8. Meneses, C. T., Duque, J. G. S., Vivas, L. G., & Knobel, M. (2008). Synthesis and characterization of TM-doped CuO (TM= Fe, Ni). *Journal of Non-Crystalline Solids*, 354(42-44), 4830-4832. <https://doi.org/10.1016/j.jnoncrysol.2008.04.025>
9. Baghdadi, N., Saeed, A., Ansari, A. R., Hammad, A. H., Afify, A., & Salah, N. (2021). Controlled nanostructuring via aluminum doping in CuO nanosheets for enhanced thermoelectric performance. *Journal of Alloys and Compounds*, 869, 159370. <https://doi.org/10.1016/j.jallcom.2021.159370>
10. Goyal, C. P., Goyal, D., K. Rajan, S., Ramgir, N. S., Shimura, Y., Navaneethan, M., ... & Ponnusamy, S. (2020). Effect of Zn doping in CuO octahedral crystals towards structural, optical, and gas sensing properties. *Crystals*, 10(3), 188. <https://doi.org/10.3390/cryst10030188>
11. Bayansal, F., Taşköprü, T., Şahin, B., & Çetinkara, H. A. (2014). Effect of cobalt doping on nanostructured CuO thin films. *Metallurgical and Materials Transactions A*, 45, 3670-3674. <https://doi.org/10.1007/s11661-014-2306-1>
12. Baturay, S., Tombak, A., Kaya, D., Ocak, Y. S., Tokus, M., Aydemir, M., & Kilicoglu, T. (2016). Modification of electrical and optical properties of CuO thin films by Ni doping. *Journal of Sol-Gel Science and Technology*, 78, 422-429. <https://doi.org/10.1007/s10971-015-3953-4>
13. Iqbal, M., Thebo, A. A., Shah, A. H., Iqbal, A., Thebo, K. H., Phulpoto, S., & Mohsin, M. A. (2017). Influence of Mn-doping on the photocatalytic and solar cell efficiency of CuO nanowires. *Inorganic Chemistry Communications*, 76, 71-76. <https://doi.org/10.1016/j.inoche.2016.11.023>
14. Sahin, B., Bayansal, F., Yüksel, M., & Çetinkara, H. A. (2014). Influence of annealing to the properties of un-doped and Co-doped CdO films. *Materials Science in Semiconductor Processing*, 18, 135-140. <https://doi.org/10.1016/j.mssp.2013.11.014>
15. Manna, S., & De, S. K. (2010). Room temperature ferromagnetism in Fe doped CuO nanorods. *Journal of Magnetism and Magnetic Materials*, 322(18), 2749-2753. <https://doi.org/10.1016/j.jmmm.2010.04.020>

16. Ortega-López, M., Avila-García, A., Albor-Aguilera, M. L., & Resendiz, V. S. (2003). Improved efficiency of the chemical bath deposition method during growth of ZnO thin films. *Materials Research Bulletin*, 38(7), 1241-1248. [https://doi.org/10.1016/S0025-5408\(03\)00083-7](https://doi.org/10.1016/S0025-5408(03)00083-7)
17. Cudennec, Y., & Lecerf, A. (2003). The transformation of Cu (OH) 2 into CuO, revisited. *Solid state sciences*, 5(11-12), 1471-1474. <https://doi.org/10.1016/j.solidstatesciences.2003.09.009>
18. Maruthupandy, M., Zuo, Y., Chen, J. S., Song, J. M., Niu, H. L., Mao, C. J., ... & Shen, Y. H. (2017). Synthesis of metal oxide nanoparticles (CuO and ZnO NPs) via biological template and their optical sensor applications. *Applied Surface Science*, 397, 167-174. <https://doi.org/10.1016/j.apsusc.2016.11.118>
19. Lu, P., Zhou, W., Li, Y., Wang, J., & Wu, P. (2017). Abnormal room temperature ferromagnetism in CuO/ZnO nanocomposites via hydrothermal method. *Applied Surface Science*, 399, 396-402. <https://doi.org/10.1016/j.apsusc.2016.12.113>
20. Manibalan, G., Murugadoss, G., Thangamuthu, R., Ragupathy, P., Kumar, R. M., & Jayavel, R. (2018). Enhanced electrochemical supercapacitor and excellent amperometric sensor performance of heterostructure CeO₂-CuO nanocomposites via chemical route. *Applied Surface Science*, 456, 104-113. <https://doi.org/10.1016/j.apsusc.2018.06.071>
21. Zamani, N., Modarresi-Alam, A. R., & Noroozifar, M. (2018). Synthesis and application of phosphorus/Co₃O₄-CuO hybrid as high-performance anode materials for lithium-ion batteries. *ACS Omega*, 3(4), 4620-4630. <https://doi.org/10.1021/acsomega.7b01153>
22. Doumeng, M., Makhlof, L., Berthet, F., Marsan, O., Delbé, K., Denape, J., & Chabert, F. (2021). A comparative study of the crystallinity of polyetheretherketone by using density, DSC, XRD, and Raman spectroscopy techniques. *Polymer Testing*, 93, 106878. <https://doi.org/10.1016/j.polymertesting.2020.106878>
23. Zargar, R. A., Arora, M., & Hafiz, A. K. (2015). Investigation of physical properties of screen printed nanosized ZnO films for optoelectronic applications. *The European Physical Journal Applied Physics*, 70(1), 10403. <https://doi.org/10.1051/epjap/2015150019>
24. Suthakaran, S., Dhanapandian, S., Krishnakumar, N., & Ponpandian, N. (2020). Hydrothermal synthesis of surfactant assisted Zn doped SnO₂ nanoparticles with enhanced photocatalytic performance and energy storage performance. *Journal of Physics and Chemistry of Solids*, 141, 109407. <https://doi.org/10.1016/j.jpccs.2020.109407>
25. Zhao, F., Hu, C., Yu, L., Li, S., Yin, M., & Fan, X. (2023). An enhanced triethylamine response by incorporating mesoporous CuO into nanosheet-assembled Co₃O₄ microtubes. *Sensors and Actuators B: Chemical*, 379, 133230. <https://doi.org/10.1016/j.snb.2022.133230>
26. Bayansal, F., Kahraman, S., Çankaya, G., Çetinkaya, H. A., Güder, H. S., & Çakmak, H. M. (2011). Growth of homogenous CuO nano-structured thin films by a simple solution method. *Journal of Alloys and Compounds*, 509(5), 2094-2098. <https://doi.org/10.1016/j.jallcom.2010.10.146>
27. Munir, A., Joya, K. S., Ul Haq, T., Babar, N. U. A., Hussain, S. Z., Qurashi, A., ... & Hussain, I. (2019). Metal nanoclusters: new paradigm in catalysis for water splitting, solar and chemical energy conversion. *ChemSusChem*, 12(8), 1517-1548. <https://doi.org/10.1002/cssc.201802069>
28. Kahraman, S., Çakmak, H. M., Çetinkaya, S., Bayansal, F., Çetinkaya, H. A., & Güder, H. S. (2013). Characteristics of ZnO thin films doped by various elements. *Journal of Crystal Growth*, 363, 86-92. <https://doi.org/10.1016/j.jcrysgro.2012.10.018>
29. Das, S., & Alford, T. L. (2013). Structural and optical properties of Ag-doped copper oxide thin films on polyethylene naphthalate substrate prepared by low temperature microwave annealing. *Journal of Applied Physics*, 113(24), 244905. <https://doi.org/10.1063/1.4812584>
30. Çetinkaya, S. (2024). Solution-based fabrication of copper oxide thin film influence of cobalt doping on structural, morphological, electrical, and optical properties. *Turkish Journal of Engineering*, 8(1), 107-115. <https://doi.org/10.31127/tuje.1290655>

